Current Science International
Volume: 10 | Issue: 04| Oct. – Dec.| 2021

EISSN:2706-7920 ISSN: 2077-4435
DOI: 10.36632/csi/2021.10.4.45
Journal homepage: www.curresweb.com
Pages: 528-542

Evaluation of Stream Sediments in Wadi Abu Furad Area, Central Eastern Desert, Egypt

Hani Hasan Ali

Nuclear Materials Authority of Egypt, P.O. Box 530, El Maadi, Cairo, Egypt

Received: 22 Sept. 2021 **Accepted:** 27 Oct. 2021 **Published:** 05 Nov. 2021

ABSTRACT

Abu Furad area lies in the Central Eastern Desert of Egypt, shows a significant widespread Precambrian outcrops including metasediments, metavolcanics, metagabbros, quartz diorite, tonalite, granodiorite and syenogranite. The stream sediments of the Wadi constitute valuable minerals categorized as radioactive minerals (uranothorite), radioactive-bearing minerals (monazite, allanite and zircon) and non-radioactive minerals (magnetite, hematite, ilmenite, leucoxene, titanite, garnet, rutile, and molybdenite) as well as green silicates. The tonnage of total economic minerals in the studied area is about 313800 ton, which is distributed as follows: about 61800 ton magnetite, about 15000 ton hematite, about 25200 ton ilmenite, about 17400 ton leucoxene, about 4800 ton garnet, about 10200 ton rutile, about 8400 ton titanite, about 18000 ton zircon, about 600 ton monazite and about 152400 ton green silicates. Mineralogical investigation integrated with statics of minerals separated from Wadi Abu Furad stream sediments show economic potentiality of these minerals which might be suitable for future exploitation. Applying typologic classification and corresponding geothermometer on the examined zircons suggest granitic origin varying from calc-alkaline series granites (Older granitoids) to sub-alkaline series granites (Younger granites and/or felsic dykes). While the plotting on the plutonic distribution diagram is mostly matching the monzonites, granodiorites, and monzogranites origin imprint. Significantly, the estimated results coincide with the main granitic exposures encountered in the study area.

Keywords: Stream sediments, Heavy minerals, Zircon typology, Abu Furad, Egypt

1. Introduction

Wadi Abu Furad study area represents a part of the Central Eastern Desert of Egypt. It is bounded by Latitudes 26º 30´ 20" - 26º 43 ´32" N and Longitudes 33º 32´ 35" - and 33º 50 ´ 27" E. Generally, the investigated area has paid the attention of several researchers' (i.e. Habib, 1982; Mahmoud, 1995; Dardier and Al-Wakeel, 1998, Esmail and Moharem 2009 and El-Mezayen *et al.,* 2019). The authors concluded that, the Abu Furad- Umm Taghir area shows a significant outcrops including migmatite, granitic gneiss, metasediment, metavolcanic, amphibolite, metagabbro and granitoid rocks. The granitic rocks composite pluton which represent the transition from the syn-orogenic granitoids (Older Granitoids) to late-orogenic granites (Younger granites). The older granitoids are classified as granodiorite, originated from metaluminous calc-alkaline magma during arc magmatism while the younger granites are originated from peraluminous cal-alkaline magma due to crustal selective anatexis during late-collision to post-orogenic magma. In the term of radioactive investigations, that the altered granites are considered uraniferous because of their relatively high U and Th contents and the main radioactive minerals are thorite, fergusonite, samarskite, columbite, zircon, monazite and xenotime. Additionally, some unzoned and zoned pegmatite pockets were recoded to show abnormal radioactive content.

Due to the different varieties of rock types encountered in the Abu Furad area, this work aims to study the stream sediments of the main Wadi to recognize and evaluate the economic heavy minerals. Also testing the zircon typology method separated from stream sediments to signify their origin based on their morphological features.

Corresponding Author: Hani Hasan Ali, Nuclear Materials Authority of Egypt, P.O. Box 530, El Maadi, Cairo, Egypt. E-mail: hanihasan1977@yahoo.com

2. Geologic outlines

The studied area is situated approximately 40 km west of Safaga City and can be reached through Qena-Safaga asphaltic road, , and toward to the south of this road into W. El-Bulla and W. Abu Furad. Generally, the study area is characterized by rugged topography due to the presence of moderate to very high mountains. The highest elevation point is represented by Gabal (G) Abu Furad younger granites (1032 m above sea level). The area is characterized by arid climatic conditions and very rarely vegetation cover.

The main basement units in the area include Precambrian exposures of metasediments metavolcanics association, metagabbros, Syn-to late-oroginic granites (quartz diorite, tonalite and granodiorite), post-oroginic granites (syenogranites), and finally dykes and veins (Fig. **1A**).

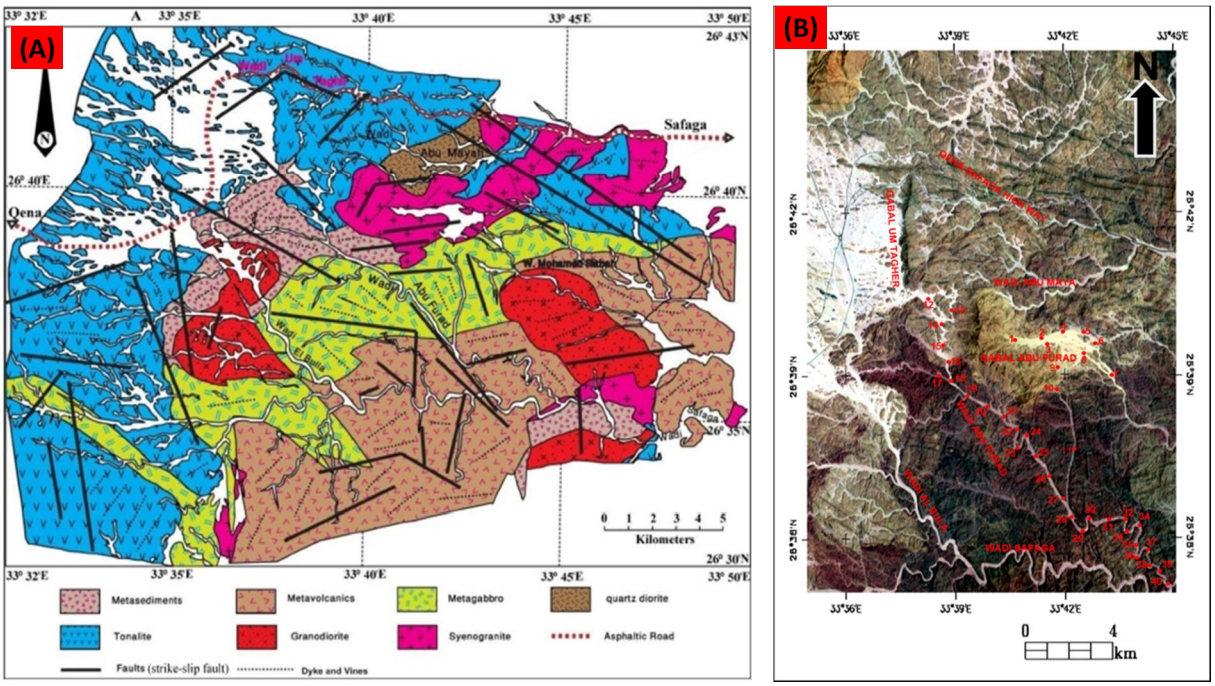

Fig. 1. (A) Geologic map of Wadi Abu Furad area, after El-Mezayen *et al.,* (2019). **(B)** Land sat image shows the distribution of sample locations.

The metasediments are represented by small belt of hornblende-schist which crop out at the southeastern and the central southwestern parts of the mapped area forming circular shape around W. El-Bulla granodiorite (Fig. 2A). The metavolcanics occupy the southeastern part of the mapped area. They are trending approximately ENE-WSW, and traversed by W. El-Bulla and W. Abu Furad and showing sharp contacts with the other surrounding rocks (Fig. 2B). On the other hand, the the metagabbros occupy the central part of the mapped area and occur as massive compact rocks of medium-to coarse-grained size and have gray color. They are of intensely jointed and fractured and show highly alteration imprints especially along the fault planes (Fig. 2B). The older granitoids represent the most predominant rock type exposed in the study area. The quartz diorite is exposed in the northeastern side of the mapped area as highly fractured and occasionally foliated rocks. The tonalite rocks occupy the western and northern parts of the mapped area along W. Mohamed Rabah intruding into the metavolcanics and metagabbros with sharp contacts. The granodiorites crop out in the southeastern part of the map around G. Umm Taghir El-Fouqani, at W. El-Bulla, and G. Abu Furad; they are intruded by syenogranites with sharp contact (Fig. 2C). Syenogranites show a limited distribution in the study area and show considerable outcrops mainly represented by the middle part G. Abu Furad at the eastern corner of the study area, and intruded into the older rocks (i.e. metasediments, metavolcanics, metagabbros, quartz diorites, tonalites and granodiorites). The Wadi Abu Furad area is injected by numerous dykes and veins of different shapes and compositions invading all the older rocks that cropping out in the study area. They have varied widths between 0.5

m and 20m and extend up to more than 20 km. These dykes are mainly of basic, intermediate and acidic in composition (Fig. 2D).

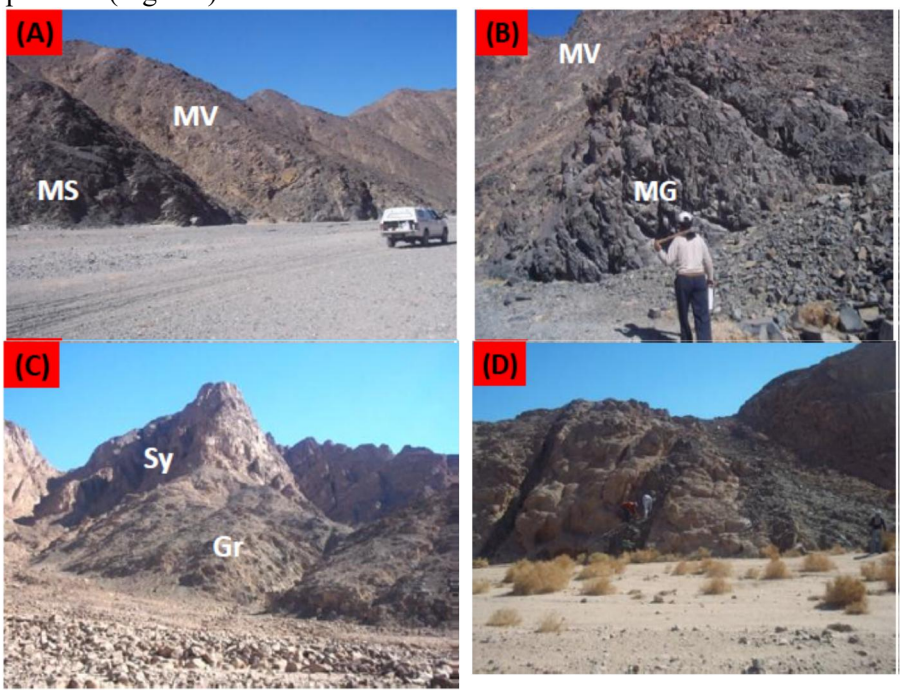

Fig. 2: (A) General view shows the sharp contact between metasediments (MS) and metavolcanics (MV) of W. Abu Furad area. **(B)** Field photograph showing the sharp contact between metgabbros (MG) and metavolcanics (MV) of W. Abu Furad area. **(C)** Field photograph showing the sharp contact between granodiorite (Gr) and syengranite(Sy). **(D)** Field photograph showing syenogranite invaded by basic dykes.

3. Materials and Methods

The samples picked by a special method depending on the nature of the study area (wadi deposits) and the samples their selves (stream sediments). A total of 40 stream sedimentary samples were collected from Wadi Abu Furad through an open bit samples of 50cm diameter and depth of one meter, the samples spacing were 500m apart (Fig. 1B). The average weight of each sample is about 10kg.

The collected samples were dried and sieved using 2mm sieve to discard gravel fractions and the rest of samples were quartered using John's Splitter and an automatic rotary splitter to obtain representative samples (about 60-80gm) for different mineralogical treatments. Each sample was sieved to get three fractions; (<800µm, 800µm-63µm and> 63µm). The size fraction ranging between 800µm-63µm for each sample weighted and subjected to decantation method to remove silt and clay particles.

Quantitative mineralogical analyses for the stream sedimentary samples were carried out by heavy liquid separation using bromoform and methylene iodide solutions (sp. gr. 2.86 g/cm3 and 3.3 g/cm3 respectively), and magnetic fractionation using a Frantz Isodynamic Magnetic Separator (Model L-1). The condition characterized Frantz Isodynamic Magnetic Separator at side slope of 5°, forward slope of 20° and step of currents 0.2, 0.5, 1.0, 1.5 magnetic and 1.5 non-magnetic current amperes.

Mineralogical investigation of the mineral constituents of the stream sediments of Wadi Abu Furad was performed through binocular stereo-microscope and Phillips XL-30 Environmental Scanning Electron Microscope (ESEM) attached by Semi-quantitative EDX microanalysis unit.

4. Heavy mineral distribution

To obtain the heavy minerals from the studied stream sediment samples, gangue minerals should be removed especially quartz and feldspars which constitute more than 80% of the stream sediments of Wadi Abu Furad by using the heavy liquid separation methods to separate the heavy minerals

fractions. The percentages of the heavy minerals content related to the original samples in the studied stream sediments were calculated and tabulated in table (1). The percentages of heavy minerals content resulted from heavy liquid separation using bromoform and methylene iodide solutions ranging from 4.56% to 17.87% and 3.28% to 7.31% with averages of 9.6% and 5.23% respectively. The high contents of the heavy minerals in the studied stream sediments are restricted in some localities near the granitic rocks.

The obtained heavy methylene iodide fractions were subjected to magnetic separation using Frantz Isodynamic Magnetic Separator (Model L-1) to fractionate heavy minerals according to their magnetic susceptibilities. First, magnetite was collected by a hand magnet, and then the magnetite free samples were subjected to the magnetic separation to produce several magnetic fractions at 0.2, 0.5, 1.0, 1.5 magnetic and 1.5 non-magnetic current amperes. Each fraction obtained from the magnetic separation process was microscopically studied under binocular stereomicroscope to investigate and calculate the frequency distribution of the concerned minerals in the studied stream sediment samples. About 1500 grains from each magnetic fraction were counted (). The weight percentage of each concerned mineral relative to the corresponding original sample was calculated according to Stakhove equation:

$Q = [P. n_m.d_m / \Sigma(n_o d_o)].100$

Where: Q = the weight percentages of the concerned mineral

P = the weight percentage of the corresponding magnetic fraction.

n_m = the number of grains of the mineral.

d_m = specific gravity of the mineral.

$\Sigma(n_o d_o)$ = the sum of the number of grains for each mineral multiplied by its specific gravity.

Table 1: Percentages of total heavy bromoform (H.Br.) and heavy methylene (H.MI.) of the studied stream sediments.

Sample No.	H.Br %	H.MI %	Sample No.	H.Br %	H.MI %
AF1	9.24	7.31	AF21	5.24	4.13
AF2	17.87	6.71	AF22	6.89	5.27
AF3	17.17	5.74	AF23	9.66	4.83
AF4	16.51	6.17	AF24	9.34	4.06
AF5	16.43	6.48	AF25	9.35	3.35
AF6	15.84	6.4	AF26	8.57	4.97
AF7	15.20	6.66	AF27	8.63	4.39
AF8	13.25	6.79	AF28	7.76	3.96
AF9	12.68	6.23	AF29	7.40	4.71
AF10	12.73	6.24	AF30	7.25	4.81
AF11	11.80	6.15	AF31	6.91	4.31
AF12	11.45	6.64	AF32	6.30	4.27
AF13	10.66	6.56	AF33	9.57	4.14
AF14	10.89	6.1	AF34	8.60	4.01
AF15	10.24	6.14	AF35	8.73	4.44
AF16	7.87	5.18	AF36	7.65	4.65
AF17	6.76	5.92	AF37	5.12	4.1
AF18	6.73	5.14	AF38	5.92	3.74
AF19	7	6.12	AF39	4.88	3.72
AF20	5.49	5.23	AF40	4.56	3.28
Max.	17.87	7.31			
Min.	4.56	3.28			
Av.	9.6	5.23			

The heavy minerals recognized microscopically are categorized to radioactive minerals (uranothorite), radioactive-bearing minerals (monazite, allanite and zircon) and non-radioactive minerals (magnetite, ilmenite, hematite, leucoxene, titanite, garnet, rutile, and molybdenite) as well as the green silicates. The percentage of each mineral related to the original samples and the average were calculated and tabulated in table (2). In the following paragraphs, the detected minerals will be displayed and described in some details.

Magnetite (Fe_3O_4) represents the major part of opaque grains of the studied samples. Magnetite displays black to deep reddish brown color, with metallic to dull luster. Their habit ranges from massive, granular, angular to sub-angular and the octahedron crystals of magnetite are less frequent and occur as isolated grains (Fig. 3A). Pure magnetite grain was investigated under the Environmental Scanning Electronic Microscope (ESEM) and the elemental chemical compositions are shown in figure (3B). Magnetite was recorded in all studied samples as common accessory mineral and its content range from 0.4% to 1.5% with an average of about 1.03%.

Table 2: Percentages of total heavy minerals in the studied stream sediments.

S. No.	Mag.	Hem.	Ilm.	Leuco.	Gar.	Rut.	Tit.	Zr.	Mz.	Gr. Si	T.H.
AF1	1.20	0.30	1.00	0.40	0.30	0.30	0.50	0.90	0.01	2.40	7.31
AF2	1.40	0.35	0.70	0.25	0.10	0.10	0.40	0.80	0.01	2.60	6.71
AF3	1.30	0.33	0.50	0.10	0.05	0.07	0.70	0.85	0.04	1.80	5.74
AF4	1.40	0.35	0.60	0.23	0.05	0.10	0.65	0.97	0.02	1.80	6.17
AF5	1.10	0.25	0.70	0.45	0.10	0.30	0.75	0.70	0.03	2.10	6.48
AF6	1.20	0.30	0.90	0.20	0.06	0.05	0.50	0.65	0.04	2.50	6.40
AF7	1.30	0.33	0.60	0.12	0.30	0.06	0.40	0.40	0.05	3.10	6.66
AF8	1.20	0.31	0.80	0.40	0.04	0.20	0.30	0.30	0.04	3.20	6.79
AF9	1.50	0.38	0.70	0.18	0.30	0.09	0.25	0.40	0.03	2.40	6.23
AF10	1.40	0.35	0.50	0.35	0.10	0.20	0.03	0.40	0.01	2.90	6.24
AF11	1.10	0.26	0.40	0.56	0.20	0.40	0.02	0.50	0.01	2.70	6.15
AF12	1.30	0.36	0.70	0.46	0.06	0.30	0.03	0.20	0.03	3.20	6.64
AF13	1.50	0.27	0.80	0.38	0.05	0.20	0.02	0.20	0.04	3.10	6.56
AF14	1.20	0.26	0.60	0.26	0.04	0.10	0.02	0.10	0.02	3.50	6.10
AF15	1.20	0.27	0.50	0.47	0.07	0.30	0.02	0.30	0.01	3.00	6.14
AF16	1.10	0.24	0.70	0.24	0.05	0.10	0.10	0.20	0.05	2.40	5.18
AF17	1.00	0.25	0.30	0.44	0.10	0.30	0.03	0.40	0.00	3.10	5.92
AF18	1.10	0.26	0.20	0.10	0.10	0.05	0.02	0.20	0.01	3.10	5.14
AF19	1.20	0.26	0.70	0.16	0.30	0.06	0.03	0.50	0.01	2.90	6.12
AF20	1.50	0.15	0.50	0.12	0.20	0.30	0.04	0.30	0.02	2.10	5.23
AF21	0.90	0.25	0.10	0.11	0.01	0.05	0.01	0.20	0.00	2.50	4.13
AF22	1.20	0.30	0.40	0.42	0.05	0.20	0.10	0.40	0.00	2.20	5.27
AF23	1.00	0.25	0.10	0.52	0.03	0.40	0.02	0.10	0.01	2.40	4.83
AF24	0.70	0.18	0.50	0.14	0.05	0.06	0.03	0.10	0.00	2.30	4.06
AF25	0.50	0.12	0.10	0.20	0.01	0.10	0.02	0.20	0.00	2.10	3.35
AF26	0.80	0.20	0.20	0.36	0.02	0.18	0.01	0.20	0.00	3.00	4.97
AF27	0.90	0.21	0.10	0.24	0.01	0.12	0.01	0.40	0.00	2.40	4.39
AF28	0.80	0.20	0.10	0.21	0.02	0.10	0.02	0.30	0.00	2.20	3.95
AF29	1.10	0.24	0.30	0.30	0.03	0.20	0.03	0.20	0.01	2.30	4.71
AF30	0.80	0.21	0.10	0.31	0.02	0.20	0.10	0.06	0.01	3.00	4.81
AF31	0.80	0.23	0.10	0.34	0.01	0.20	0.02	0.10	0.01	2.50	4.31
AF32	0.70	0.18	0.20	0.22	0.02	0.21	0.03	0.10	0.01	2.60	4.27
AF33	0.50	0.12	0.10	0.45	0.04	0.20	0.20	0.02	0.01	2.50	4.14
AF34	1.00	0.25	0.20	0.20	0.04	0.10	0.10	0.01	0.01	2.10	4.01
AF35	0.90	0.21	0.30	0.35	0.01	0.30	0.02	0.05	0.00	2.30	4.44
AF36	1.00	0.25	0.20	0.57	0.02	0.40	0.04	0.07	0.00	2.10	4.65
AF37	0.90	0.22	0.30	0.11	0.04	0.05	0.02	0.06	0.00	2.40	4.10
AF38	0.70	0.19	0.30	0.13	0.03	0.06	0.03	0.10	0.00	2.20	3.74
AF39	0.50	0.12	0.40	0.14	0.05	0.07	0.04	0.10	0.00	2.30	3.72
AF40	0.40	0.10	0.10	0.24	0.01	0.10	0.10	0.03	0.00	2.20	3.28
Min.	0.40	0.10	0.10	0.10	0.01	0.05	0.01	0.01	0.00	1.80	3.28
Max.	1.50	0.38	1.00	0.57	0.30	0.40	0.75	0.97	0.05	3.50	7.31
Aver.	1.03	0.25	0.42	0.29	0.08	0.17	0.14	0.30	0.01	2.54	5.23

S. No. = Sample number, Mag. = Magnetite, Hem. = Hematite, Ilm. = Ilmenite, Leuco. = Leucoxene, Gar. = Garnet, Rut. = Rutile, Tit. = titanite, Zr. = Zircon, Mz. = Monazite, Gr. Si. = Green Silicates, T.H. = Total heavy.

Hematite (Fe_2O_3), is the principle ore of iron which originated mainly from magnetite alteration processes and alteration product of many Fe-bearing minerals especially pyrite and so called hematite after pyrite (goethite) or pseudomorphic pyrite (Fig. 3C). Hematite occurs as massive, granular and

angular to sub angular grains with dull luster and displays reddish brown to reddish black color (Fig. 3D). Hematized pyrite grain was investigated under the Environmental Scanning Electronic Microscope (ESEM) and the elemental chemical compositions are shown in figure (3E). Hematite was recorded in all studied samples as common accessory mineral and its content range from 0.1% to 0.38% with an average of about 0.25%.

Ilmenite ($FeTiO_3$), is the most common Fe-Ti oxide mineral that occurs in a wide variety of igneous rocks, some metamorphic rocks and as detritus mineral grains. It exhibits iron-black color with metallic luster and occurs as massive, granular, nearly rounded and tabular grains (Fig. 3F and G). Pure ilmenite grain was investigated under the Environmental Scanning Electronic Microscope (ESEM) and the elemental chemical compositions are shown in figure (3H). Ilmenite was recorded in all studied samples as common accessory mineral and its content range from 0.1% to 1.0% with an average of about 0.42%.

Leucoxene (mixture of Fe-Ti oxides) is not a mineral but it represents the transitional phase during the alteration of ilmenite to form the secondary rutile (Mohamed, 1987, Mohamed, 1998 and Elsner, 2010). It displays rounded to subrounded grains with smooth or pitted surface ranging in color from yellow to yellowish brown and dark brown (Fig. 3I). Ilmenite occurs as relicts on the surface of leucoxene as indications of alteration processes. Pure leucoxene grain was investigated under the Environmental Scanning Electronic Microscope (ESEM) and the elemental chemical compositions are shown in figure (3J). It was recorded in the all studied samples as common accessory mineral and its content ranges from 0.1% to 0.57% with an average of about 0.29%.

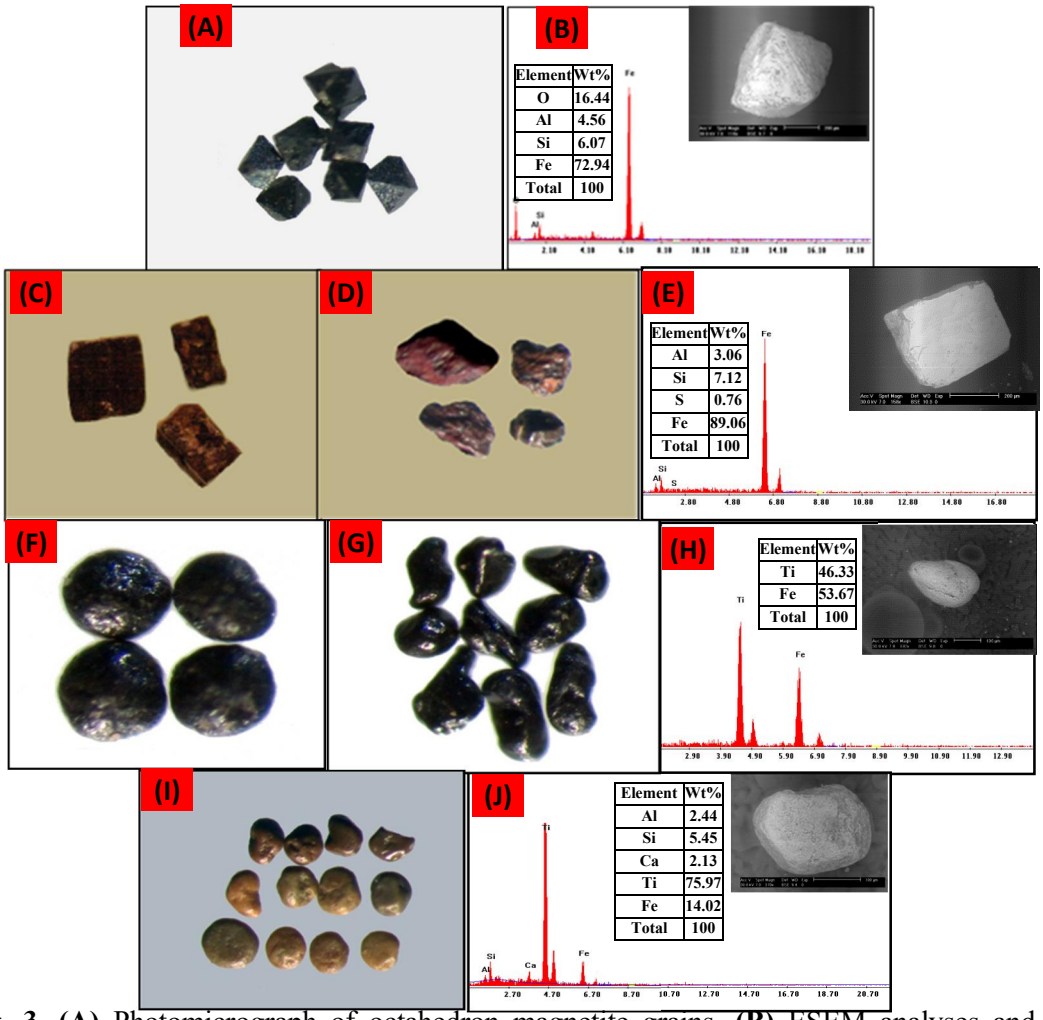

Fig. 3. (A) Photomicrograph of octahedron magnetite grains. **(B)** ESEM analyses and BSE. **(C)** Photomicrograph of hematized pyrite. **(D)** Granular and angular to sub-angular grains of hematite. **(E)** ESEM analyses of hematized pyrite with BSE. **(F and G)** Photomicrographs of rounded granular and tabular grains of ilmenite. **(H)** ESEM analyses with BSE. **(I)** Photomicrograph of rounded to subrounded grains of leucoxene. **(J)** ESEM analyses and BSE.

Titanite (Ca Ti Si O_5) is of widespread in acidic, intermediate igneous rocks and in several metamorphic rocks as accessory phase. It occurs as subhedral to euhedral grains of adamantine luster and imperfect cleavage exhibiting transparent to translucent yellow to yellowish brown color (Fig. 4A). Pure titanite grain was investigated under the Environmental Scanning Electronic Microscope (ESEM) and the elemental chemical compositions are shown in figure (4B). It was recorded in the all studied samples as common accessory mineral and its content ranges from 0.01% to 0.75% with an average of about 0.14%.

Zircon ($ZrSiO_4$) represents the main accessory mineral in the present study which dominates in all samples especially in non-magnetic fractions exhibit wide variety in color and morphology. In the term of zircon morphological features as well as internal structures, The examined zircons come in a variety of colors, including colorless (water clear zircon), light yellow, brilliant yellow, honey, brown, dark brown, reddish brown and reddish black (Fig. 4C), with some crystals exhibiting significant overgrowth. The most frequent form of zircon is doubly-terminated prismatic crystals with elongation ratios (length-to-width) from 1 to 5 (Corfu *et al.,* 2003). Elongation is seen in some of the zircon grains examined (Fig. 4C), indicating a significant fluid content in the magma and validating the magmatic origin (Pupin *et al.,* 1978; Dardier, 1999; El-Mansi *et al.,* 2004; Omran and Dessouky 2016). Zircon xenocrystic core occurs simply when a previously crystallized zircon is surrounded by later crystallized one, possibly generated during late-stage crystallization; the older zircon becomes a xenocrystic core in the newly formed zircon. When a previously crystallized zircon is surrounded by a later crystallized zircon, presumably created during late-stage, the older zircon transforms into a xenocrystic core in the freshly formed zircon. The studied zircon exhibit significant xenocrystic cores feature (Figs. 4C and D). Zircon was recorded in the all studied samples as common accessory mineral and its content ranges from 0.01% to 0.97% with an average of about 0.3%.

Garnet is generally considered as characteristic mineral of metamorphic rocks as well as being found in some granites and acid volcanic rocks (Deer *et al.,* 1992). In the present study, garnet occurs as subhedral to anhedral grains of solid solution ranging in color from rose, orange and deep orange with vitreous luster (Fig. 4E). Pure almandine-spessartine garnet grain was investigated under the Environmental Scanning Electronic Microscope (ESEM) and the elemental chemical compositions are shown in figure (4F). It was recorded in the all studied samples as common accessory mineral and its content ranges from 0.01% to 0.3% with an average of about 0.08%.

Monazite [(Ce, La, Nd, Th) PO4] is one of the most important nuclear minerals, being a major host for REEs and actinides Th and U (Hinton and Paterson 1994, Bea *et al.,* 1994& Bea 1996). It is widely disseminated in granitic rocks and schistose metamorphic rocks as well as the detrital sediments and typically associated with zircon and titanite. In the present study, monazite occurs as subrounded to oval grains ranging in color from colorless to pale yellow with vitreous luster (Fig. 4G). Pure monazite grain was investigated under the Environmental Scanning Electronic Microscope (ESEM) and the elemental chemical compositions are shown in figure (4H). It was recorded in 62% of the studied samples as common accessory mineral and its content ranges from 0.01% to 0.05% with an average of about 0.01%.

Rutile (TiO_2) is the preferred mineral for the production of titanium dioxide and occurs as an accessory mineral in many types of igneous rocks, some metamorphic rocks under high pressure and temperature conditions and as detrital mineral grains. Rutile occurs as subhedral prismatic, tabular and elongated form ranging in color from deep blood red to black with adamantine luster (Fig. 5A). Pure rutile grain was investigated under the Environmental Scanning Electronic Microscope (ESEM) and the elemental chemical compositions are shown in figure (5B). It was recorded in all studied samples as common accessory mineral and its content ranges from 0.05% to 0.4% with an average of about 0.17%.

Allanite [$(Ca, Ce, La)_2$ $(Al, Fe^{3+}, Fe^{2+})_3$ O. SiO_4. Si_2O_7. OH] is a rather uncommon accessory mineral in granites, granodiorites, syenites, nepheline syenites, and similar light-colored, plutonic igneous rocks, where it is usually associated with epidote and iron-rich ferromagnesian silicates, and it is a rare accessory in schists and gneisses (Phillips and Griffen, 1981). In the studied samples, allanite presents as subhedral to anhedral grains with submetallic luster. The allanite grains are brownish black to black in color (Fig. 5C). Pure allanite grain was investigated under the

Environmental Scanning Electronic Microscope (ESEM) and the elemental chemical compositions are shown in figure (5D).

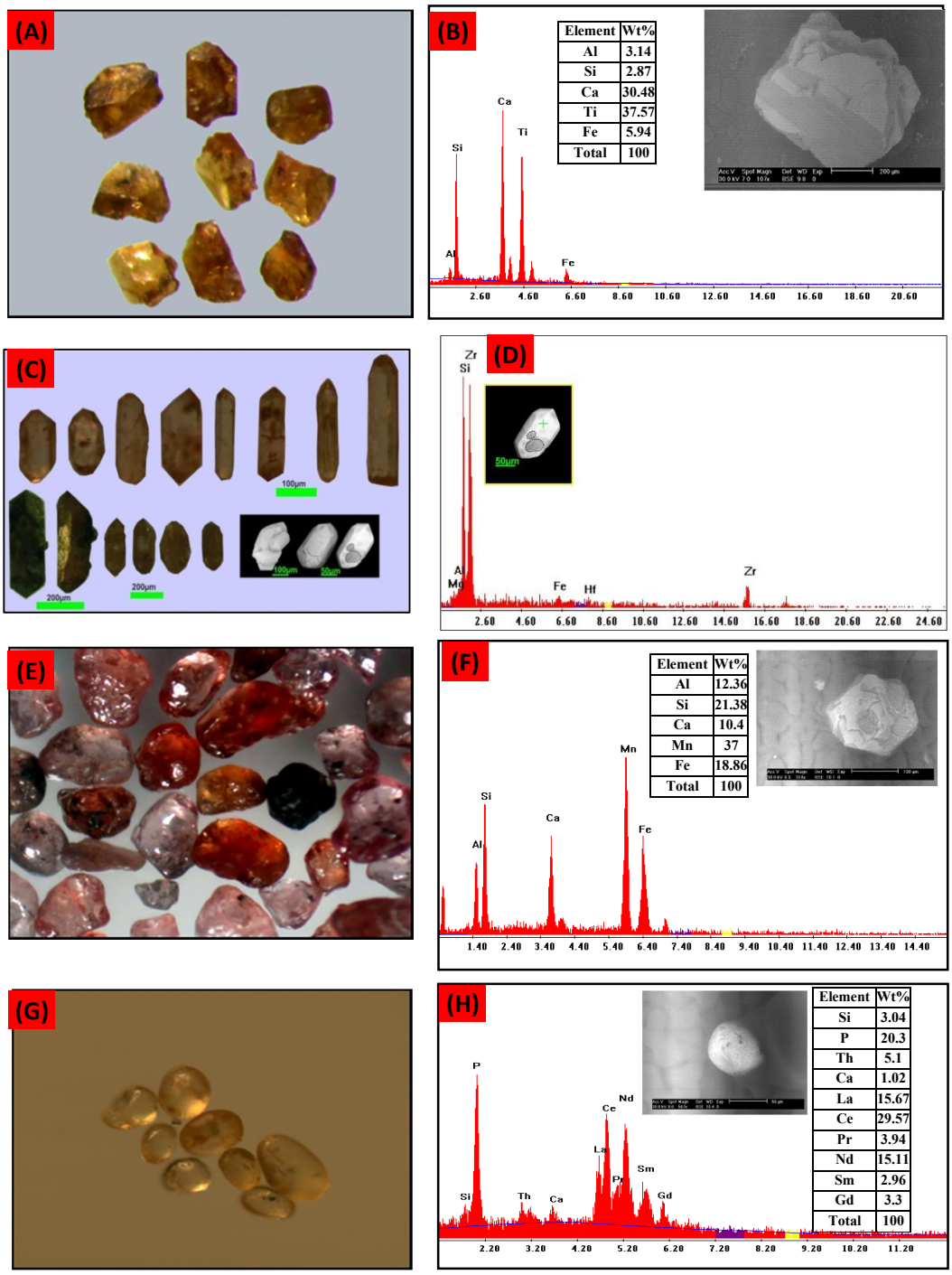

Fig. 4. **(A)** Photomicrograph of subhedral to euhedral grains of titanite **(B)** ESEM analyses and BSE**. (C)** Acompined of photomicrograph and BSE of different types of separated euhedral zircon grains from different stream samples**. (D)** Example of SEM analyses of the studied zircon with BSE of zircon show xenocrystic core. **(E)** Photomicrograph of subhedral to anhedral garnet grains. **(F)** ESEM analyses and BSE **(G)** Photomicrograph of subrounded to oval monazite grains. **(H)** ESEM analyses and BSE.

Uranothorite [(Th, U) SiO_4] is the most abundant uranium and thorium mineral which is a variety of thorite minerals rich in uranium. It is isomorphous with zircon and strongly radioactive (Frondel, 1958). In the studied samples, uranothorite occur as subhedral to anhedral grains ranging in color from yellowish brown to brown with vitreous and resinous luster (Fig. 5E). The uranothorite

grains are highly mitamicted. Metamictization leads to their crystal lattice destruction as a result of its own radiation effect. The effect can destroy a crystal lattice completely while leave the outward appearance unchanged. Pure allanite grain was investigated under the Environmental Scanning Electronic Microscope (ESEM) and the elemental chemical compositions are shown in figure (5F).

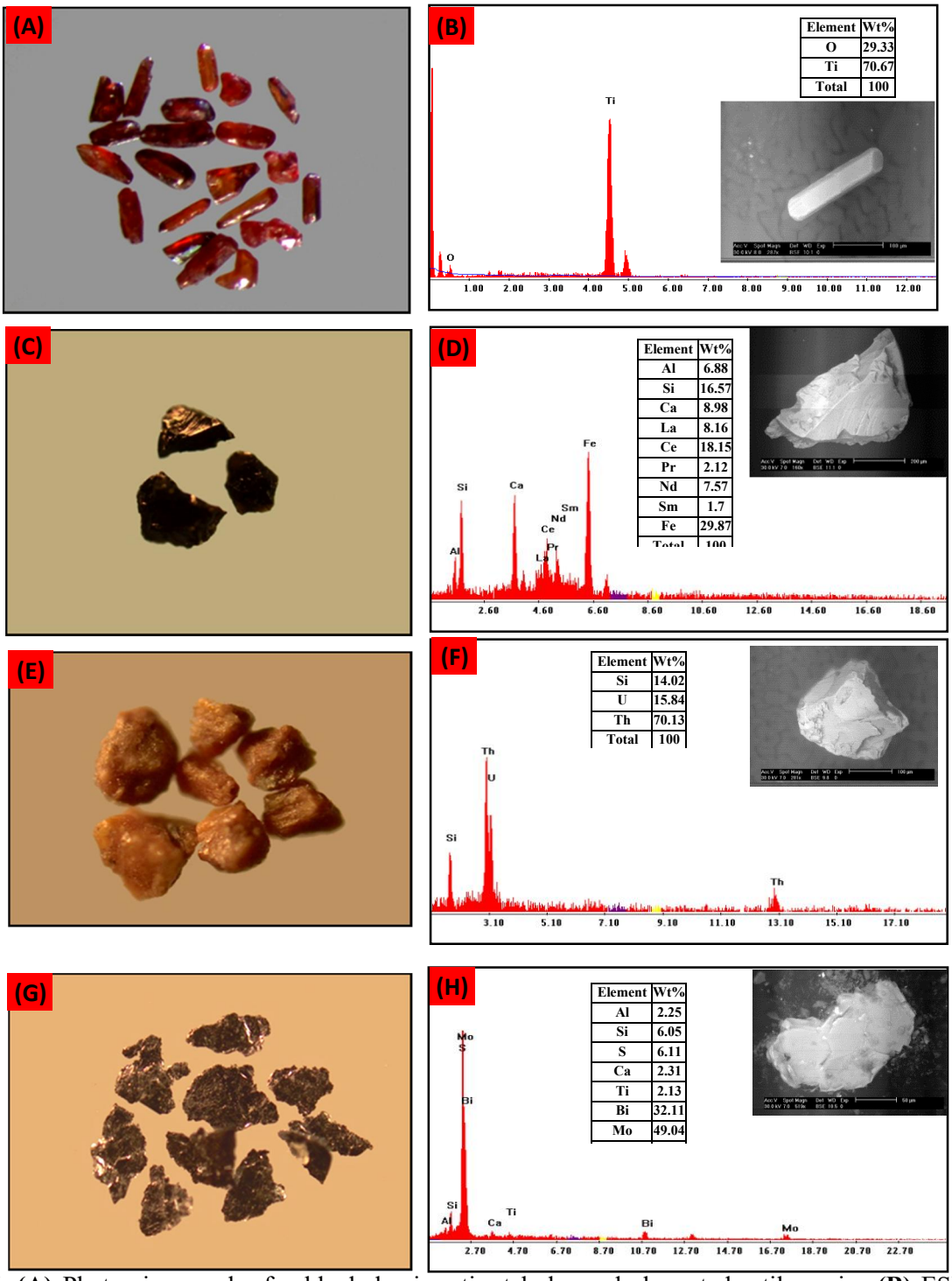

Fig. 5. (A) Photomicrograph of subhedral prismatic, tabular and elongated rutile grains **(B)** ESEM analyses and BSE. **(C)** Photomicrograph of allanite grains **(D)** ESEM analyses and BSE. **(E)** Photomicrograph of subhedral to anhedral uranothorite grains **(F)** ESEM analyses and BSE. **(G)** Photomicrograph of platy molybdenite grains. **(H)** ESEM analyses and BSE.

Molybdenite (MoS_2) is the most important source of molybdenum which occurs in granite, pegmatite and hydrothermal veins. In the present study, molybdenite exhibits gray to lead-silvery gray

flexible platy grains with metallic luster (Fig. 5G). Pure allanite grain was investigated under the Environmental Scanning Electronic Microscope (ESEM) and the elemental chemical compositions are shown in figure (5H). The EDX data indicate the presence of Bi (32.11%).

5. Evaluation of the study area

The volume of raw sand of the top meter in the studied area is calculated by multiplying the length x width x of stream sediments. The tonnage of the raw sand of these sediments is calculated by multiplying the volume of the raw sand by the specific gravity of the sediments as shown in table (3). The tonnage of the total economic minerals was calculated by multiplying the tonnage of the raw sand (ton) by average calculated weight percentage of total economic minerals (Table 4). The tonnage of the individual economic mineral was calculated by the tonnage of the raw sand (ton) by average calculated weight percentage of individual economic mineral divided by 100 (Table 5).

Table 3: The tonnage of the raw sand of the studied area.

Volume (m^3) Length x width x depth	Specific gravity of the raw sand (ton/m^3)	Tonnage of the raw sand (ton)
20000x200x1 = 4000000	1.5	6000000

Table 4: The tonnage of the total economic minerals in the studied area.

Tonnage of the raw sand (ton)	The average weight percent of total economic heavy minerals	The average reserve of total economic minerals (ton)
6000000	5.23	313800

Table 5: The tonnage of the individual economic minerals in the studied area.

Economic mineral	The average weight percent of economic heavy minerals	The average reserve of individual economic minerals (ton)
Magnetite	1.03	61800
Hematite	0.25	15000
Ilmenite	0.42	25200
Leucoxene	0.29	17400
Garnet	0.08	4800
Rutile	0.17	10200
Titanite	0.14	8400
Zircon	0.3	18000
Monazite	0.01	600
Green Silicates	2.54	152400
Total	5.23	313800

6. Zircon typology

Zircon usage as a likely clue for identifying the granite origin has been proposed by Poldervaart since 1950; and did now no longer receive wide acceptance due to the fact the proposed standards of dimensional crystal statistics didn't produce the preferred solution. Regarded to Pupin (1980), the chemistry, water content, and temperature and cooling rate of the melt all influence the formation of zircon distinct crystal faces (Pupin, 1985). The zircon typology method proposed by Pupin (1980) basically arrangement of morphological types of zircon on the zircon typologic diagram based on the relative development of {100} and {110} prisms and {101} and {211} pyramids (Fig. 6).Based on his scheme, I-type granites (Older Granitoids) are showing zircon crystals with flat pyramids {1 0 1} whereas S-type granites mainly have zircon crystals with steep pyramids {2 1 1} (Pupin, 1980; Finger *et al.,* 1991, 1992; Schermaier *et al.,* 1992; Benisek and Finger, 1993; Sturm, 1999; Belousova *et al.,* 2006; Köksal *et al.,* 2008). Also, the chemical composition of the magma, specifically the aluminum/alkali ratio (A), controls the development of zircon pyramids whereas the crystallization temperature mange the formation of the different zircon prisms (Pupin, 1980).

Here, the zircon typology method (Pupin, 1980), based on the external morphology of zircon crystals was applied on zircons separated from six samples. These samples were chosen to test the typology method on the detrital zircons which isolated form stream sediments adjacent to nearby granitoid masses of the study area.

Binocular and SEM images of zircons from the different studied stream sediment samples are summarized in figure (7); profound changes of the external zircon crystal morphology are recognizable as would be expected for genetically different granitoid types encountered in the study area. Accordingly, the analyses of those zircons indicate major types which are S24, S20, S15, P2 and P5. While the types of S5, S25, P1 and P4 are less dominant. S14 and S19 types are present in minor amount in the studied samples (Table 3 and Fig. 7).

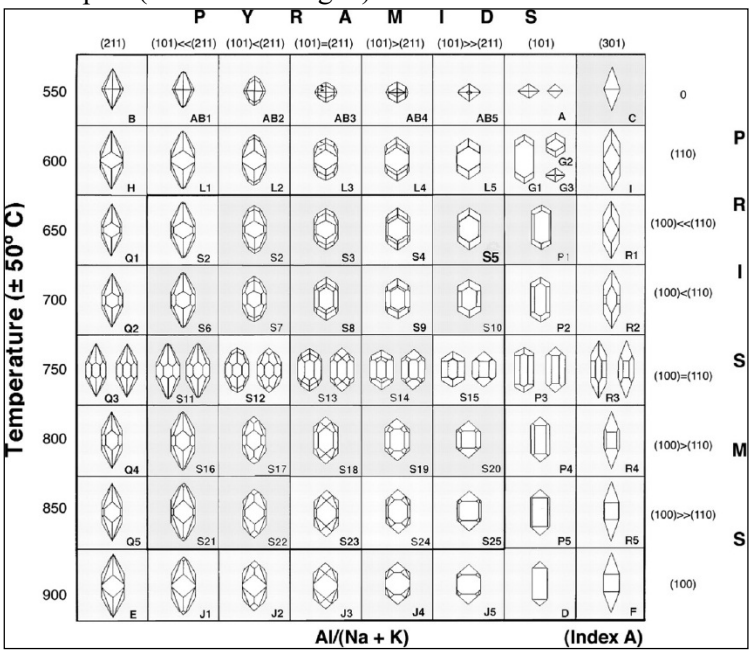

Fig. 6: Zircon typological classification and corresponding geothermometric scale proposed by Pupin (1980). Index A reflects the Al/alkali ratio, controlling the development of zircon pyramids, whereas temperature affects the development of different zircon prisms.

Table 6: Statical calculations and zircon distribution frequency based on Pupin (1980) of the studied zircon population.

	S5	S20	S24	S25	S15	P1	P2	P4	P5
Sample 1	37	39	47	28	6	10	13	14	4
Sample %	24	25	22	14	3	7	2	2	2
T	71	148	152	99	15	21	6	12	14
A	142	148	109	85	18	49	11	14	14
Sample 2	22	33	31	21	23	22	17	-	16
Sample %	11	17	16	11	12	11	9	-	8
T	34	101	153	75	59	34	34	-	57
A	67	101	109	64	70	78	60	-	57
Sample 3	45	34	48	25	65	4	9	8	6
Sample %	16	12	17	9	24	1	3	3	2
T	49	74	203	63	118	4	13	17	15
A	98	74	145	54	141	10	23	20	15
Sample 4	53	3	22	-	33	-	12	3	7
Sample %	40	2	17	-	25	-	9	2	5
T	134	14	116	-	124	-	36	14	37
A	239	14	83	-	18	-	63	16	37
Sample 5	14	5	47	27	33	19	10	5	9
Sample %	8	3	28	16	20	11	6	3	5
T	25	18	203	112	98	34	24	18	37
A	50	18	145	96	117	79	41	21	37
Sample 6	-	19	47	53	23	4	10	5	12
Sample %	-	11	27	31	13	2	6	3	7
T	-	66	28	214	66	7	23	17	49
A	-	66	136	184	80	16	40	20	49

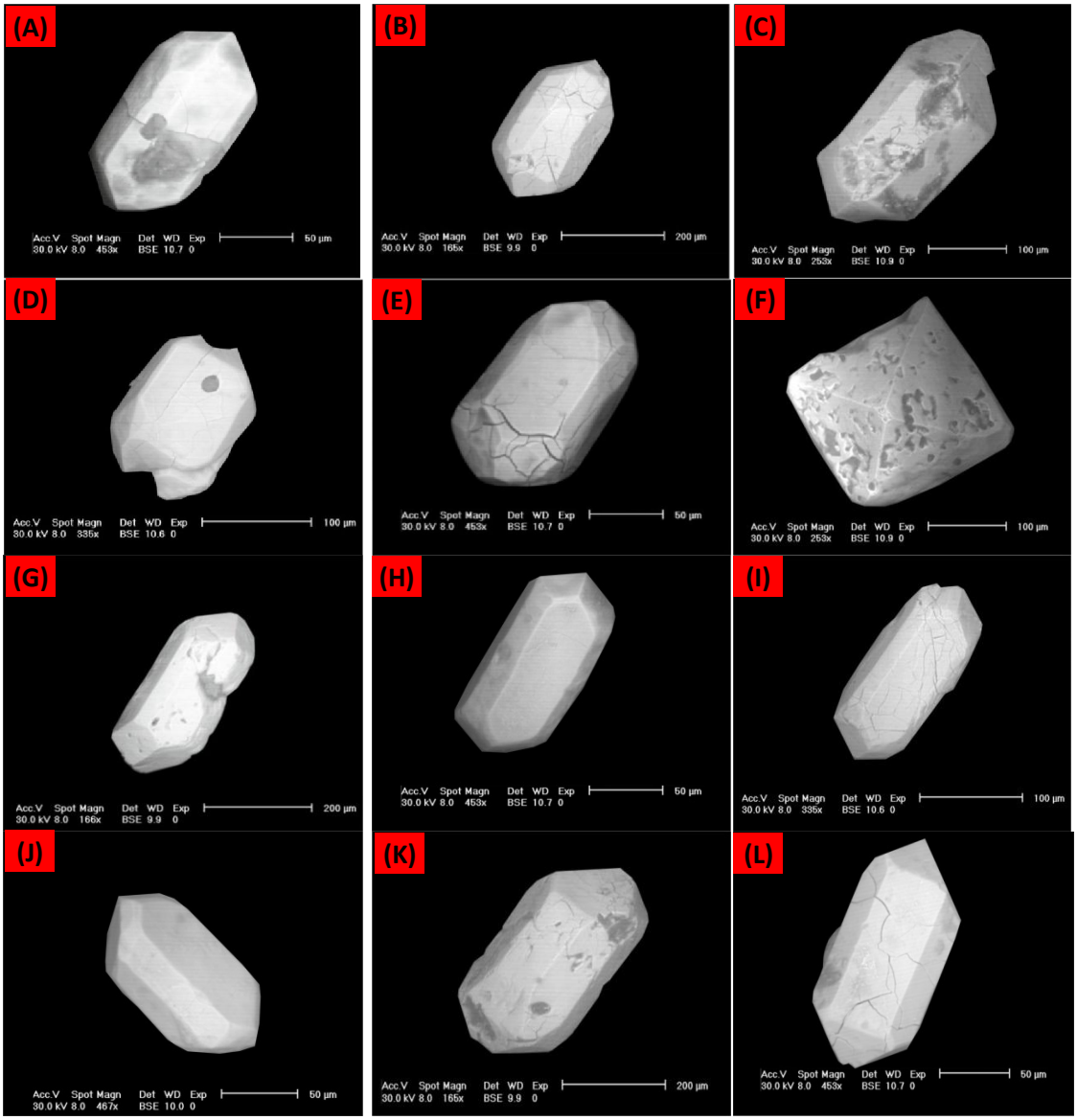

Fig. 7: Crystal morphology characteristics of zircon (SEM) from different samples of the studied stream sediments. **A-F** zircon crystals category showing the development of pyramid and prism which are belong to S24, S20, S5, S25, S19,and S25. **G-I** zircon crystals category showing the development of pyramid and prism which are belong to P1, P2, P4and P5.

The typologic distribution has been determined and the coordinates in I.A. and I.T. (temperature index) space are computed (Pupin, 1980), for the chosen six samples I.A. (1)= 591, I.A. (2) = 606, I.A. (3) = 681, I.A. (4) = 469, I.A. (5) = 604 and I.A. (6) = 591 with average I.A. ≈ 594.8 and I.T. (1)= 539, I.T. (2)=545, I.T. (3)=557 , I.T. (4)=473, I.T. (5)=567, and I.T. (6)=471 with average I.T. ≈ 525.3 (Figs. 8A-F). The results of mean point of the investigated zircon grains from stream sediments are plotted on the diagrams (Figs. 8G and H). Morphology of the studied zircon crystals suggests that, all of zircon crystals belong to granitic source. Particularly, samples (1, 3, 4 and 6) matching the calc-alkaline series granites (i.e. Older granitoids). Whereas, the samples (2 and 5) belong to sub-alkaline series granites (i.e. Younger granites and/or felsic dykes). While on the distribution of plutonic rocks in the typologic diagram; all of samples matching the granodiorites, monzogranites and monzonites origin imprint (Fig. 8H).

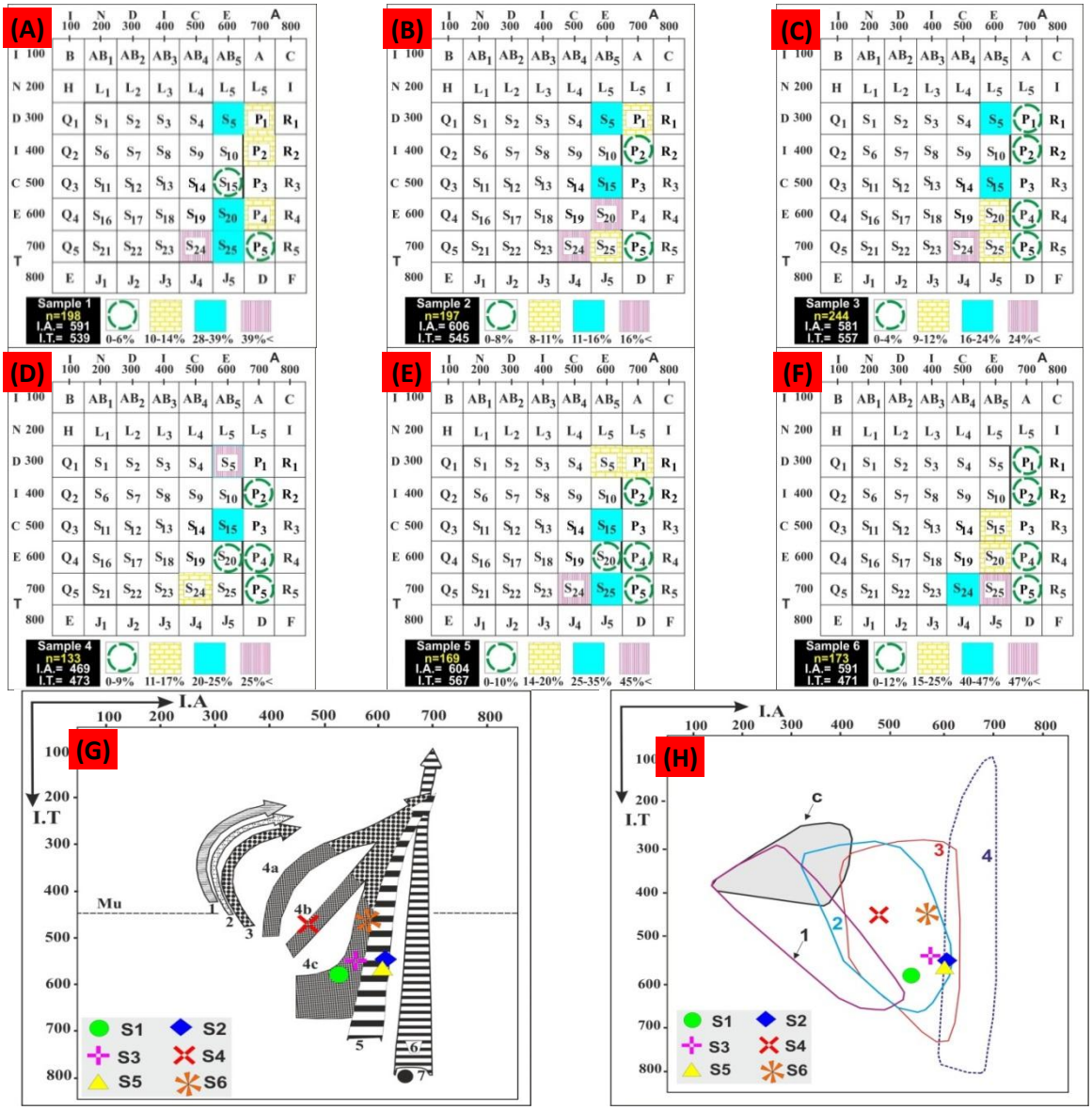

Fig. 8: A-F Typologic frequency distribution of separated zircons from stream sediments in the study area, n = the number of investigated zircon crystals. **(G)** Distribution of mean points and mean typological evolutionary trends of zircon populations (Pupin, 1980) from: Aluminous anatectic granites (1) aluminous leucogranites; (2) (par) autochthonous monzogranites and granodiorites; (3) intrusive aluminous monzogranites and granodiorites. –Hybrid granites of crustal + mantle origin: (4a, b, c) calc-alkaline series granites (dark doted area = granodiorites +monzogranites; clear doted area = monzogranites + alkaline granites); (5) sub-alkaline series granites; (6) alkaline series granites ;(7) tholeiitic series granites. -Mu = limit of the muscovite granites (I.T = 450). **(H)** Distribution of plutonic rocks in the typologic diagram: (1) diorites, quartz gabbros and diorites, tonalites; (2) granodiorites ; (3) monzogranites and monzonites; (4) alkaline and hyperalkaline syenites and granites; (c) cordierite bearing rocks.

5. Conclusion

Wadi Abu Furad area is bounded by Latitudes 26º 30´ 20" - 26º 43 ´32" N and Longitudes 33º 32´ 35" - and 33º 50 ´ 27" E covered by 40 representative stream sediment samples. The main rock units exposed in Wadi Abu Furad area were chronologically arranged as metasedimets, metavolcanics and metagabbro which comprises the metamorphic rocks; quartz diorite, tonalite and granodiorite which comprises the older granites and syenogranite which comprise the younger granite. The heavy minerals recognized microscopically are categorized to radioactive minerals (uranothorite),

radioactive-bearing minerals (magnetite, hematite, ilmenite, leucoxene, titanite, garnet, rutile, and molybdenite) as well as the green silicates.

The heavy minerals recognized microscopically as magnetite, ilmenite, hematite, leucoxene, titanite, zircon, garnet, rutile, monazite, allanite, uranothorite and molybdenite beside the green silicates. The calculated percentages of these minerals related to the original samples are: magnetite which ranging from 0.4% to 1.5% with an average of about 1.03%, hematite ranging from 0.1% to 0.38% with an average of about 0.25%, ilmenite ranging from 0.1% to 1.0% with an average of about 0.42%, leucoxene ranging from 0.1% to 0.57% with an average of about 0.29%, titanite ranging from 0.01% to 0.75% with an average of about 0.14%, zircon ranging from 0.01% to 0.97% with an average of about 0.3%, garnet ranging from 0.01% to 0.3% with an average of about 0.08%, monazite ranging from 0.01% to 0.05% with an average of about 0.01%, rutile ranging from 0.05% to 0.4% with an average of about 0.17% and green silicates ranging from 1.8% to 3.5% with an average of about 2.54%.

The tonnage of total economic minerals in the studied area is about 313800 ton, which is distributed as follows: about 61800 ton magnetite, about 15000 ton hematite, about 25200 ton ilmenite, about 17400 ton leucoxene, about 4800 ton garnet, about 10200 ton rutile, about 8400 ton titanite, about 18000 ton zircon, about 600 ton monazite and about 152400 ton green silicates. Mineralogical investigation integrated with statics of minerals separated from Wadi Abu Furad stream sediments show economic potentiality of these minerals which might be suitable for future exploitation.

Morphology of the studied zircon crystals suggests that, all of zircon crystals belong to calc-alkaline series granites (Older granitoids) and sub-alkaline series granites (Younger granites and/or felsic dykes). While on the distribution of plutonic rocks in the typologic diagram; all of samples matching the granodiorites, monzogranites and monzonites origin imprint.

References

Bea, F., 1996. Residence of REE, Y, Th and U in granites and crustal protolith; implications for the chemistry of crustal melt. J. Petrol., 37: 521:552.

Bea, F., M.D. Pereira, L.G. Corretage and G.B. Fershtater, 1994. Differentiation of strongly peraluminous, perphosphorous granites: the Pedrobenards pluton, Central Spain. Geochemica et Cosmochemica Acta, 58: 2609:2627.

Belousova, E.A., W.L. Griffin and S.Y. O'Reilly, 2006. Zircon crystal morphology, trace element signatures and Hf isotope composition as a tool for petrogenetic modeling: examples from eastern Australian granitoids. Journal of Petrology, 47: 329–353.

Benisek, A. and F. Finger, 1993. Factors controlling the development of prism faces in granite zircons- a microprobe study. Contribution to Mineralogy and Petrology, 114 (2): 441–451.

Corfu, F., J.M. Hanchar, P.W.O. Hoskin and P. Kinny, 2003. Atlas of zircon textures. In: Hanchar JM, Hoskin PWO (eds) Zircon. Reviews in mineralogy and geochemistry, 53: 469–500.

Dardier, A.M., 1999. Morphology and geochemistry of zircon associated with uranium mineralization in Gattar granitic pluton, north Eastern Desert, Egypt. Jour. Mineral. Soc. Egypt, 11: 91-104.

Dardier, A.M. and M.I. Al-Wakeel, 1998. Geology, petrology and radioactivity of Gabal Um Tagher - Gabal Abu Furad area, Central Eastern Desert, Egyp. Egyptian Journal of Geology, the Geological Society of Egypt, Cairo, 42: 75-103.

Deer, W.A., R.A. Howie and J. Zussman, 1992. An introduction to the rock-forming minerals. (Second edition). ELBS with Longman. 696.

El-Mansi, M.M., A.M. Dardier and I.M. Abdel Ghani, 2004. Crystal habit and chemistry of zircon as a guide for uranium redistribution in Gabal Ria El-Garrah area, Eastern Desert, Egypt. Delta Jour. Of Sci., 28: 19- 30.

El-Mezayen, A.M., E.K. Abu Zeid, W.S. Hosny, M.G. El-Feky, S.M. Omar, and S.A. Taalab, 2019. Geochemistry, mineralogy, and radioactivity of the Abu Furad Area, Central Eastern Desert, Egypt. Acta Geochim, 38(2): 307–326.

El-Mezayen, A.M., M.G. El-Feky, M.O. Sayed and S.A. Ibrahim, 2015. Geochemistry and a composite M-type with W-type of REE tetrad effect in altered granites of Abu Furad area, Central Eastern Desert, Egypt. Greener J. Geol. Earth Sci., 3(2):013–029.

Elsner, H., 2010. Heavy minerals of economic importance. Assessment manual, Faculty of Geosciences of the University of Hannover: 218p. 31 Fig. 125 Tab.

Esmail, E.M. and A.F. Moharem, 2009. Fluid inclusion studies of radioactive mineralized pegmatites at Gabal Abu Furad area, central Eastern Desert, Egypt. JKAU Earth Science, 21: 1-13.

Finger, F., G. Friedl and B. Haunschmid, 1991. Wall-rock derived zircon xenocrysts as important indicator minerals of magma contamination in the Freistadt granodiorite pluton, northern Austria. Geologica Carpathica, 42 (2): 67–75.

Finger, F., B. Haunschmid, A. Schermaier and A. Von Quadt, 1992. Is zicon morphology indicative of a mantle or crustal origin of a granite? Comparison of Pupin indices with Sr and Nd isotop data of 26 Austrian granites. Mitt. Österr. Mineral. Ges., 137: 135–137.

Frondel, C., 1958. Systematic mineralogy of uranium and thorium. U. S. Geol. Survey Bull. 1064: 160-170.

Ghobrial G.A., and M.H. Girgis, 1982. Granitoid rocks of Wadi El-Bullah area, Eastern Desert, Egypt. Egypt J. Geol., 26:107–120.

Habib M.E., 1982. Landsat investigation of mineralized granites in the area between G. El-Urf and G. El-Erediya areas West of Safaga, Egypt. In: Proceedings of 8th later symposium. Burchue university, 15.

Hinton, R.W. and B.A. Paterson, 1994. Crystallization history of granitic magma: evidences from trace elements zoning. Mineral. Mag., 58A: 416:417.

Köksal, S., M. Göncüoglu, F. Toksoy-Köksal, A. Möller, and H. Kemnitz, 2008. Zircon typologies and internal structures as petrogenetic indicators in contrasting granitoids types from central Anatolia, Turkey. Mineralogy and Petrology, 93:185–211.

Mahmoud F.O., 1995. Geology and radioactivity of Abu Furad-Umm Taghir area, Eastern Desert, Egypt. M.Sc. thesis, Geological Department, Faculty of Science (Qenq)—South Valley University, 141.

Mohamed, E.H., 1987. Mineralogical studies for some Quaternary sediments in northern Sinai. M. Sc. Thesis, Ismailia Univ.

Mohamed, S.S.M., 1998. Radioactivity and mineralogic studies on wadi Abu Dabbab alluvial deposits, Central Eastern Desert, Egypt. M. Sc. Thesis, Fac. of Sci., Ain Shams Univ. 204p.

Omran, A.A. and O.K. Dessouky, 2016. Ra's Abdah of the north Eastern Desert of Egypt: the role of granitic dykes in the formation of radioactive mineralization, evidenced by zircon morphology and chemistry. Acta Geochim. 354, 368–380.

Phillips, W.R. and D.T. Griffen, 1981. Optical mineralogy, the non-opaque minerals. Freeman and Company, Sanfrancisco, U.S.A.

Poldervaart, A., 1950. Variation of optical properties with composition in the Forsterite-Fayalite series. American Mineralogist, 35(11-1): 1067-1079.

Pupin, J.P., 1980. Zircon and granite petrology. Contributions to Mineralogy and Petrology, 73(3), 207-220.

Pupin, J.P., 1985. Magmatic zoning of Hercynian Granitoids in France based on zircon typology. Schweizerische Mineralogische und Petrographische Mitteilungen, 65: 29–56.

Pupin, J.P., B. Bunin, M. Tessier, and G. Turco, 1978. Role de I'cau sules caracteres morphologiques, et la cristallisation du zircon dans les granitoides. Bull. Soc. Geo. Fr., 20: 721-725.

Schermaier, A., B. Haunschmid, G. Schubert, G. Frasl, and F. Finger, 1992. Diskriminierung von S-Typ und I-Typ Graniten auf der Basis zirkontypologischer Untersuchungen. Frankfurter Geowiss. Arb., Serie A Geologie-Paläontologie, 11: 149–153.

Sturm, R., 1999. Longitudinal and cross section of zircon: a new method for the investigation of morphological evolutional trends. Schweizerische Mineralogische und Petrographische Mitteilungen, 79: 309–316.